Materials Science & Engineering C 108 (2020) 110386

Contents lists available at ScienceDirect

Materials Science & Engineering C

journal homepage: www.elsevier.com/locate/msec

# Cancer-targeted and intracellular delivery of Bcl-2-converting peptide with functional macroporous silica nanoparticles for biosafe treatment

Yuehuang Wu[1], Pengjin Ge[1], Weixia Xu, Mingyu Li, Qi Kang, Xiaokun Zhang, Jingjing Xie*

*School of Pharmaceutical Sciences, Fujian Provincial Key Laboratory of Innovative Drug Target Research, Xiamen University, Xiang'an South Road, Xiamen, Fujian, 361102, China*

ARTICLE INFO

*Keywords:*
Macroporous silica nanoparticles
Targeted delivery
Bcl-2-converting peptide
Cancer treatment
Folate receptor

ABSTRACT

Therapeutic peptide, NuBCP-9 (N9) as a Bcl-2 functional converter, has been demonstrated to have the remarkable anticancer efficiency in Bcl-2-abundant cancer. However, it faced technical challenges in clinical use, such as the low bioavailability, the easily-destroyed bio-stability, and the insusceptibility to cellular interior. With the potential of mesoporous silica nanoparticles (MSNs) as the promising delivery vehicle of therapeutic macromolecules, we developed a kind of MSNs with the surface coating of folic acid (FA) for cancer cell targeting and with the macropore loading of N9 peptide for cancer therapy. Our results showed that the functional MSNs had the relatively greater biosafety than the naked MSNs in zebrafish models, leading to less than 30% embryo of death at 200 μg/ml, which could further specifically target the folate receptor (FR)-overexpressed cervical cancer HeLa cells instead of FR-negative normal embryonic kidney HEK 293T cells in a FA-competitive manner. N9 peptide with the delivery of functional MSNs could be internalized by HeLa cells, and co-localized with mitochondria in a Bcl-2-dependent manner. Moreover, N9 peptide delivered by FA-modified MSNs displayed the excellent anticancer efficiency with great selectivity, inducing approximately 52% HeLa cells into apoptosis. In summary, our results illustrated the potential of functional MSNs with large pore size as an efficient nanocarrier for the intracellular delivery of peptide drugs with targeting proteins to realize cancer therapy.

## 1. Introduction

The increasing cancer incidence and mortality rates make the prevention, diagnosis and targeted therapy become badly urgent. There are two main obstacles to the successful cancer treatment: the severe toxic side effects and the cancer multidrug resistance (MDR) [1]. One of the causes for cancer MDR is the anti-apoptotic protein such as B cell lymphoma gene 2 (Bcl-2) [2]. Bcl-2 family proteins are important regulators of the anti-apoptotic machinery and the mitochondrial outer membrane potential (MOMP) [3]. The anti-apoptotic activity of Bcl-2 has been targeted by small drug molecules such as ABT-137, navitoclax, Apogossypol, HA-14, anti-ycin A, Oblimersen sodium, Gossypol (AT-101), ab-737 (ab-263), GX15-070, VENCLEXTA, etc., which are all in the FDA approved clinical application or in trial [4]. Although many Bcl-2 targeted drugs have been developed or are being developed, they mainly inhibit the anti-apoptotic function of Bcl-2 by releasing the Bcl-2 gene as a Bcl-2 inhibitor [5].

Nur77 (also known as TR3 or NGFI-B) is a potent member of the nuclear receptor superfamily that promotes apoptosis and can be transferred from the nucleus to the mitochondria of different death signals under stimuli [6]. NUBCP-9 (N9) is a short Nur77-derived peptide containing 9 amino acids. It acts as a molecular recognition switch that converts Bcl-2 from protectors to cancer killers by binding to Bcl-2 loop, eliminating BH4 domain, exposing to BH3 domain, and triggering a conformational change in Bcl-2. Its unique property is that N9 not only antagonizes the function of Bcl-2 and induces Bcl-2 conformation to be transformed into a BH3-like molecule, but also inhibits the survival function of its anti-apoptotic relatives such as Bcl-XL [6]. In contrast with chemotherapeutics, therapeutic peptides targeting intracellular protein displayed the superior anticancer efficiency with great biosafety. However, the preclinical development of peptidyl drugs for cancer treatment is extremely obstructed by their instability, poor pharmacological properties, low bioavailability and poor cell penetrative capabilities *in vivo* [3]. The development of state-of-art nanomedicines based on mesoporous silica nanoparticles (MSNs) is expected to overcome the above difficulties in the application of peptidyl drugs (e.g., N9). That's because MSNs are generally recognized as safe by FDA and used as one of the most promising drug delivery carriers. Due to the

* Corresponding author.
*E-mail address:* xiejj@xmu.edu.cn (J. Xie).
[1] These authors contributed equally to this work.

https://doi.org/10.1016/j.msec.2019.110386
Received 7 September 2019; Received in revised form 13 October 2019; Accepted 30 October 2019
Available online 05 November 2019
0928-4931/ 

tunable particle size (10-1000 nm) and pore diameter (2-20 nm) in wide ranges, and the facile surface functionalization [7], MSNs nanocarriers have a distinctively high payload of anti-cancer drugs and controllable release feature, and can be easily modified with targeting (e.g., folic acid, FA) and "stealth" molecules (e.g., polyethylene glycol, PEG) [8] to be the smart bombs. However, the conventional MSNs usually possessed the small pore sizes, thus it is usually difficult to load the large molecules. Moreover, it is a slow process to diffuse bio-macromolecules through pores < 5 nm [9]. In sharp contrast, we have synthesized the MSNs with small sizes of < 50 nm and large enough pore channels of > 5 nm to transport the Bcl-2 functionally transformed peptides into mitochondria of tumor cells [10].

Folate receptors (FR), a glycophosphatidylinositol-linked cell surface receptor, as the targets are usually over-expressed on the surface of most solid tumor cells and relatively low-expressed on normal cells [11]. Therefore, many scientific experiments on utilizing FA (or other substances similar to FA) as a targeting ligand molecule to modify the drug delivery vector for achieving the specific localization of tumor cells *in vivo* and releasing the anticancer drugs to kill cancer cells have been reported [12,13]. In this study, we presented an exciting strategy to achieve the dual targeting outcomes by modifying the large pore sized-MSNs surface with FA as the active targeting ligand and encapsulating a Bcl-2-converting peptide (N9) as a mitochondria targeting agent [14]. The effective loading of N9 will be achieved through the macropores of MSNs, and the specific targeting FR-positive tumor cells to avoid toxicity will be obtained by the FA binding of MSNs surface. The cell toxicity and apoptosis assays of N9 peptide were also carried out in FR-positive human cervical cancer HeLa cells and FR-negative human embryonic kidney HEK293T cells, and the biosafety of MSNs nanocarriers was investigated in zebrafish models. This study will provide a strategy for dual targeting tumor therapy with Bcl-2 polypeptides via the design of functional macroporous silicon-based nanomaterials.

## 2. Results

### 2.1. Characterization of well-ordered MSNs with FA functionalization and peptide loading

The N9 peptide was reported to play the apoptosis-inducing function via targeting mitochondria and converting Bcl-2 conformation, so a small enough particle size is an important prerequisite for MSNs delivering peptide to the designated mitochondrial position. The large pore sized- and small particle sized- MSNs were synthesized as we previously reported [10]. Dynamic light scattering (DLS) measurement showed that the average hydrodynamic diameter of MSNs in pure water was 108 nm corresponding to 0.18 g triethanolamine (TEA) (Fig. 1H). Both scanning electron microscopy (SEM) and transmission electron microscopy (TEM) analyses displayed that the synthesized MSNs had the average particle size of 33 nm while possessed the approximately spherical morphology with the dendrimer-like mesoporous internal structure (Fig. 1A, D). When the surface was modified with amine functionality/targeting moiety or the pore was encapsulated with peptide drugs, there was no obvious change in surface morphology and particle size (Fig. 1B, C, E). But if N9 peptide was conjugated onto MSNs-FA surface, there was a bit of increase in particle size (36 nm) as shown in Fig. 1F. The DLS measurement also confirmed the successful surface functionalization at each step, accompanied by the surface charge of MSNs was from negative (-32.8 ± 0.95 mV) to positive (29.9 ± 0.51 mV), then to positive (23.0 ± 1.94 mV) (Fig. 1G). When dispersed in dd$H_2O$, though MSNs had the uniform size distribution, the DLS diameter was increased from 108.1 ± 0.55 nm to 143.1 ± 4.52 nm after surface was decorated with FA molecules (Fig. 1H and I). The hydrophilic diameter seemed to be larger than the SEM diameter, which might be due to the aggregation phenomenon because of the hydrate layers on the particle surface. Nitrogen adsorption-desorption isotherm measurement further demonstrated that MSNs possessed the relatively low specific surface areas of 137-151 $m^2/g$ and pore volume of 0.4-0.6 ml/g, but the large well-defined pore size of 10-15 nm, indicating their macroporous characters (Fig. 1J-L). Relative to the conventional MSNs with small pore size (< 5 nm) [15,16], our prepared MSNs had the macropore size, which would contribute to the enhanced loading of Bcl-2-converting peptide, even other macromolecules, such as nucleic acid and protein drugs.

### 2.2. Verification of the surface functionalization and peptide release

To confirm the synthesis of peptide-delivered MSNs-targeted delivery system, various techniques were used. The signal resonating between 6.59 and 8.66 ppm were largely assigned to the characteristic aromatic protons on FA from the surface of MSNs, which further confirmed the successful functionalized silica (Fig. S1). The successful functionalization of MSNs with FITC and decoration with Rhodamine B-labeled N9 (i.e., N9-RB) could also be demonstrated from the unique fluorescence images of the green and red colors from N9-RB@FITC-MSNs-FA in pure water (Fig. 1M and N). The loading efficiency of N9 was 8.2% (wt%). The *in vitro* release studies showed that there wasn't a pH-sensitive release behavior of FITC-labeled N9 peptide (i.e., N9-FITC) from the pores of MSNs-FA. As shown in Fig. 1 O, the release behavior was displayed with a typical three-phase character containing a burst release before 10 h, followed by a slow release over 48 h, then a steady release over 96 h. It was found that 10.62% and 16.33% of N9 were respectively released by 10 h and 96 h when the nanoparticles were incubated in PBS at pH 7.4, whereas, only 0.18% and 1.49% were released at pH 5.0. The initial burst release of peptide before 10 h might be attributed to the presence of N9-FITC peptides absorbed on the surface of the MSNs-FA nanoparticles. Moreover, the lack of acid-responsive release characteristics of peptide from the macropores of MSNs-FA nanoparticles, consistent with previously reported [3], might be related to the theoretical isoelectric point (PI = 9.76) of N9 peptide, which would largely contribute to its less degradation and enhanced stability in cells.

### 2.3. Selective cell-targeting and internalization of functional nanoparticles mediated by folate receptor

N9 peptide could be attached on the surface of MSNs or be encapsulated into the macropores of MSNs. To compare the cell-penetration capability of peptide with the aid of MSNs in different carrying ways, the cellular internalization behaviors were accordingly investigated under a laser confocal microscope. After 3 h of incubation, we found that N9 peptide could be taken by MSNs-FA into cytoplasm of HeLa cells in N9-loading way instead of conjugating way (Fig. S2). Thus, N9 peptide was prone to be loaded into the macropores of MSNs for the following experiments. In order to verify the feasibility of targeted drug delivery carriers for the effective cancer targeting and cellular internalization, FA-modified MSNs were attached with fluorescein to provide a means for fluorescent tracing. FR-negative HEK293T and -positive HeLa cells were both used to show the target specificity of MSNs-FA in this assay. After exposed to MSNs-FA nanoparticles for different times (0, 1, 3, 6, 12 h), cells were labeled with mitotracker and DAPI for taking fluorescence images. The result showed that in the first 3 h, no or less green fluorescence color was observed from the cells, indicating that the incubation time is not enough for MSNs penetrating cell membrane. With the incubation time prolonged, MSNs-FA could specifically bind HeLa cell membrane at 6 h, then penetrate the cell membrane into cytoplasm and distribute in mitochondria, especially after 12 h (Fig. 2A, C). The co-localization of particle with mitochondria was demonstrated by the merged green-red fluorescence color. The reason why MSNs-FA nanoparticles were distributed in mitochondria might be attributed to the FA/FR-mediated endocytosis effects. However, similar phenomenon wasn't found in HEK293T cells even at 12 h

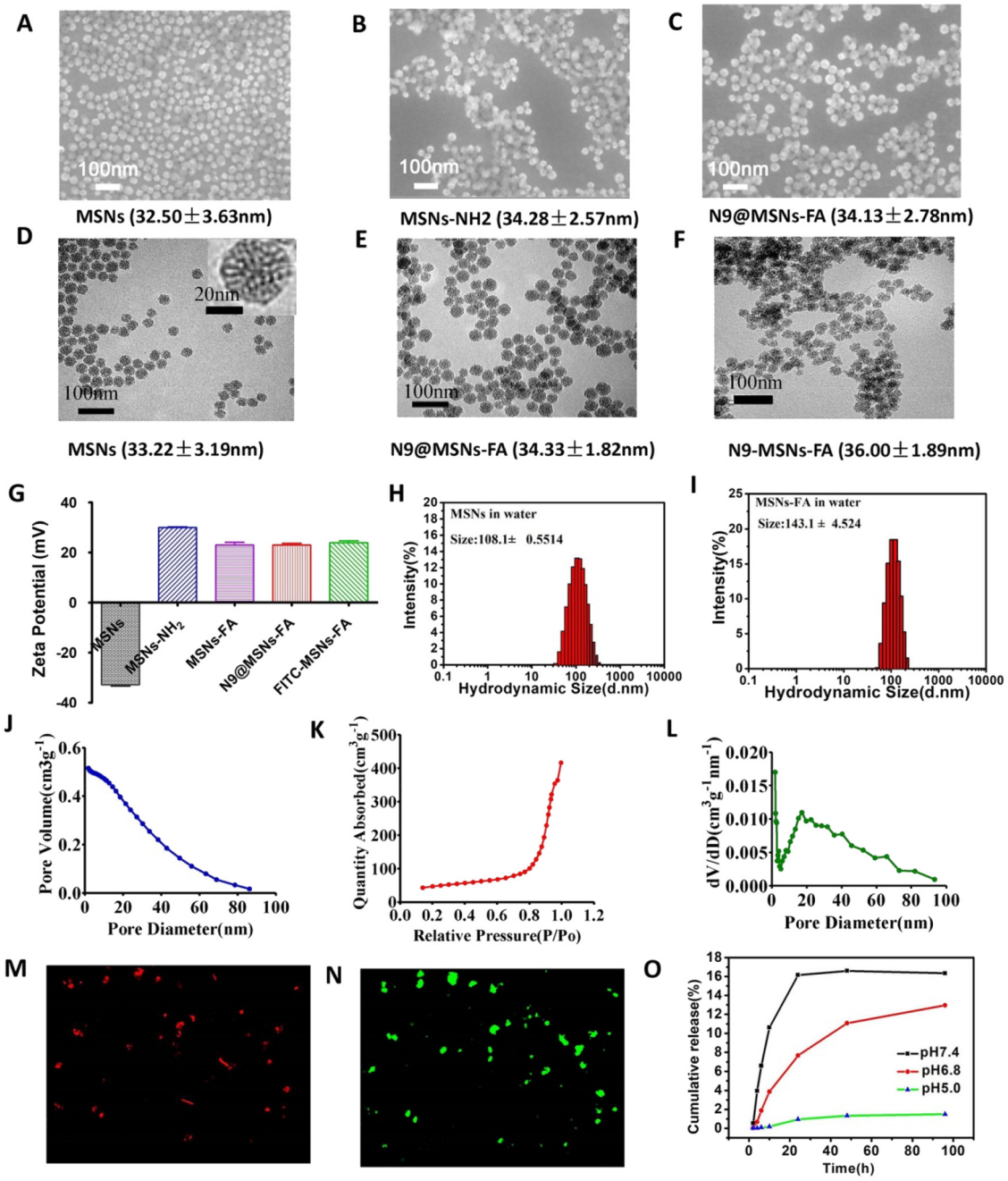


**Fig. 1.** Physicochemical characterization of FA-modified macroporous silica nanoparticles (MSNs) encapsulated with N9 peptide. The morphological and zeta potential changes of MSNs before and after a series of surface functionalization and loading with N9 peptide analyzed both by SEM (A,B,C) and DLS (G,H,I). Confirmation of MSNs (D) encapsulated with (E) or attached with (F) N9 peptide by TEM images. Nitrogen desorption isotherms displaying the distribution of pore size and pore volume of MSNs (J,K,L). Fluoresence images confirming FITC-labeled MSNs-FA nanoparticles (M) encapsulated with RB-labeled N9 peptide (N) in pure water. Cumulative release curves of N9 peptide from the pores of MSNs-FA nanoparticles at different pH values (O).

(Fig. 2B). It seemed that HeLa cancer cells were more prone to be bound by FA-modified MSNs than HEK293T, which was up to the over-expression level of folate receptor on cancer cells not on normal cells. The obtained results demonstrated that the introduction of FA ligand could significantly improve specific targeting of MSNs to HeLa cells over HEK293T normal cells, thereby facilitating the N9 peptide endowed by target cells and released to the mitochondrial location for the following cell apoptosis function.

In order to confirm the FR-mediate endocytosis of functional MSNs, HeLa cells were treated with FA prior to FITC labeled-MSNs-FA incubation. The flow cytometry experiment was carried out to quantify the mean fluorescence intensity from HeLa cells. Without FA competition, the binding capacity of MSNs-FA was increased with the incubation time prolonged from 3 h to 24 h, which was determined by the improved fluorescence intensity of FITC from cells. The cellular uptake efficiency reached about 85% after 24 h of incubation, which was calculated based on the percentage of FITC-positive cells (Fig. 2D). However, in the presence of free FA, the decreased fluorescence intensity or the reduced percentage of FITC-positive cells was observed, about by 10%-20%, demonstrating an inhibition of cellular uptake by free FA (Fig. 2D). The FR competition experiments further confirmed the specific FR-mediated targeting of MSNs-FA for FR-positive cancer cells.

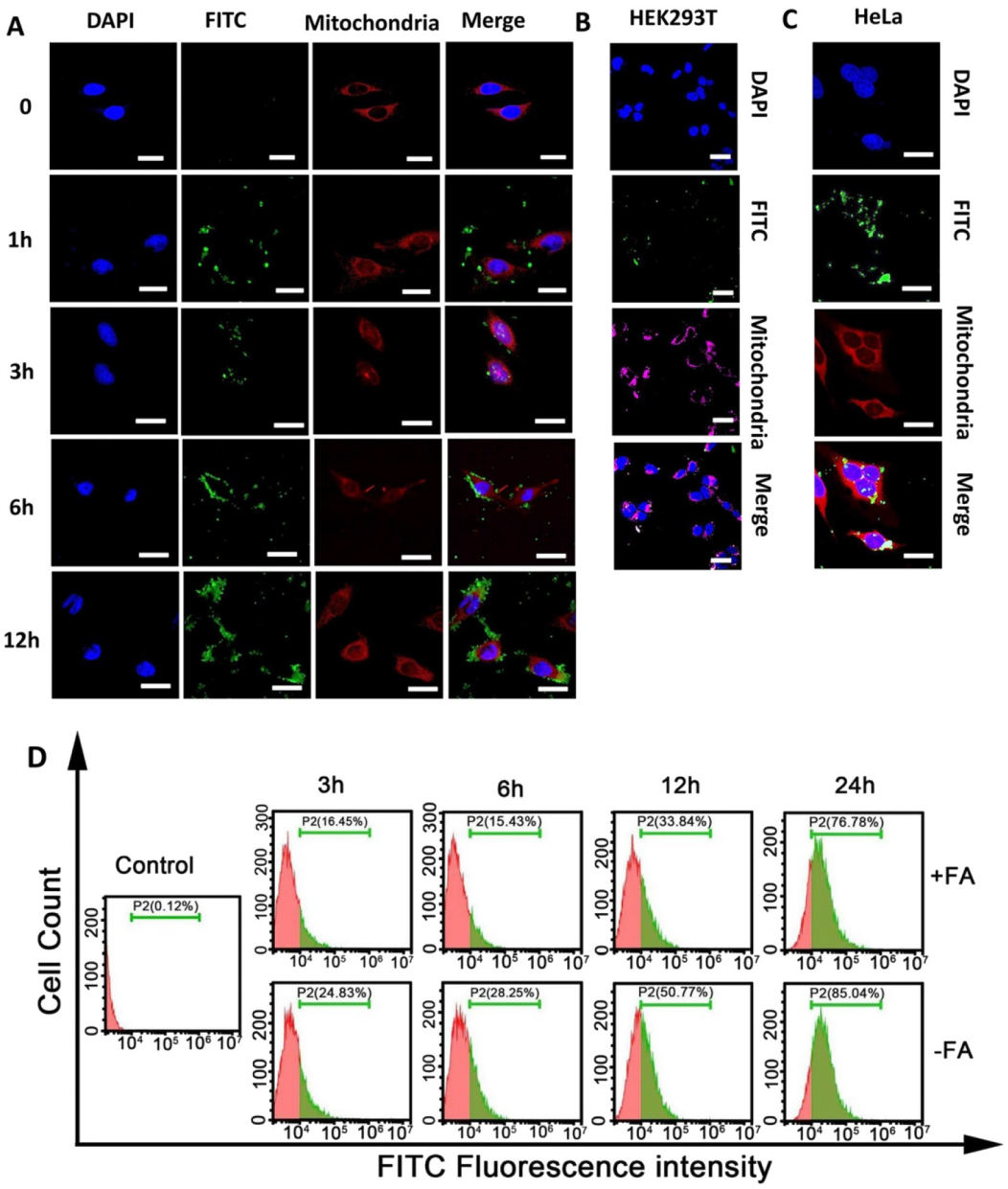


**Fig. 2.** LSCM and FACS analyses of cell targeting and cell internalization behaviors mediated by FITC-labeled MSNs-FA nanoparticles. A, Penetration and internalization behaviors of FITC-MSNs-FA in HeLa cancer cells with incubation time prolonged from 1 h to 12 h. B-C, Selective targeting and internalization behaviors of FITC-MSNs-FA nanoparticles in FR-negative HEK293T (B) and FR-positive HeLa (C) cells after 12 h of their co-incubation. DAPI (blue) and mitochondrial probe (deep red) were respectively used to show the presence of cell nucleus and mitochondria. Note, scale bar: 25 μm. D, Flow cytometric analysis of the competitive cellular uptake behaviors mediated by FA in different time intervals. HeLa cells were treated with or without 1 mM FA for 30min, followed by FITC-MSNs-FA incubation for different times. (For interpretation of the references to color in this figure legend, the reader is referred to the Web version of this article.)

### *2.4. Time course-dependent cell endocytosis, uptake and mitochondrial localization of peptide*

Accumulation on cellular mitochondria is the necessary prerequisite for the apoptosis function of N9 peptide. In view of this, flow cytometry was carried out to compare the delivery efficiency of N9@MSNs-FA into FR-negative (HEK293T) and -positive (HeLa) cells. As shown in Fig. S3, MSNs-FA nanoparticles and N9 peptide could be selectively taken up by HeLa not HEK293T cells, and their cellular uptake efficiencies respectively reached 22.7% and 3.3% compared to the control cells based on the percentage of FITC- and RB- positive cells. Microscopic analysis was then performed on HeLa cells to investigate the capacity of MSNs-FA delivering N9 peptide to the designated mitochondrial position.

Given that the binding of N9 with Bcl-2 protein on mitochondrial was the key point for converting Bcl-2 from a protector to a killer of cancer cells, the studies on the co-localization of N9-loaded MSNs-FA with mitochondria and the endogenous Bcl-2 were respectively evaluated in this assay. Confocal microscope analysis was made after HeLa cells treatment with N9@MSNs-FA for 12 and 24 h followed by mitotracker labeling or immunofluorescence staining of the intracellular protein Bcl-2. The images displayed that the merged yellow-fuchsia fluorescence predicted a high level of co-localization between N9@MSNs-FA (yellow) and Bcl-2 (fuchsia). With the incubation time prolonged from 12 h to 24 h, a significant binding between N9@MSNs-FA and Bcl-2 was observed and the internalization of nanoparticles to cell nucleus was even found from the merged fluorescence color (yellow-blue). Thus, the synthesized N9@MSNs-FA showed the relatively great cell-penetration capacity, which was consistent with what we

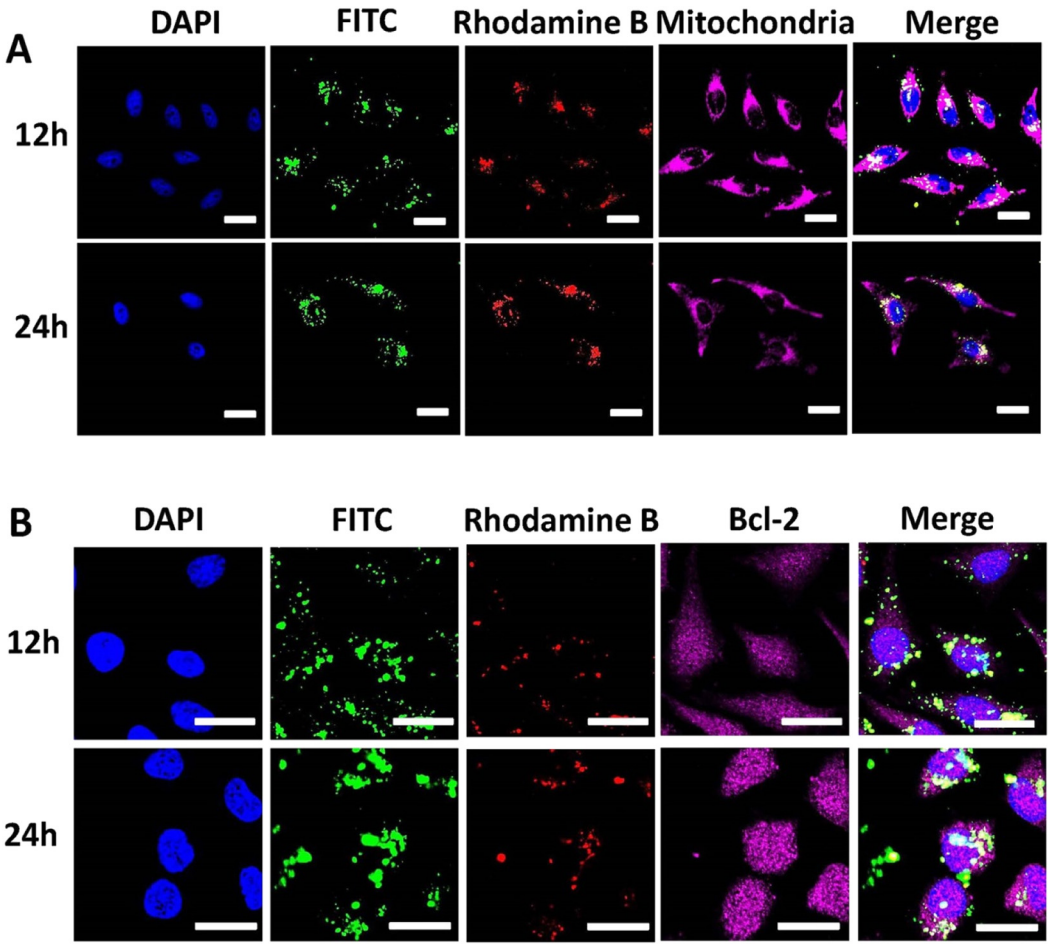


**Fig. 3.** Microscopic analysis of the co-localization behaviors of fluorescence-labeled N9@MSNs-FA with mitochondria (A) or Bcl-2 protein (B) in HeLa cells after 12 h or 24 h of co-incubation, respectively. Note, the green and red fluorescence colors, respectively, indicated the presence of MSNs-FA nanoparticles and N9 peptide within cells. Scale bar: 25 μm. (For interpretation of the references to color in this figure legend, the reader is referred to the Web version of this article.)

previously reported [10]. Taken together, these observations will contribute to the induction of apoptosis by N9. Especially at 12 and 24 h, the N9 peptide could be effectively delivered to mitochondria accompanied by MSNs-FA nanoparticles, which was the result of the fluorescence overlap between green (MSNs), red (N9), and deep-red (mitochondria) spots (Fig. 3A).

As a Bcl-2 converter, N9 peptide derived from a Nur77 fragment needs to interact with Bcl-2 and expose BH3 domain to make the pro-apoptosis function. So whether N9 targeted mitochondria by binding Bcl-2 was further investigated by us. Immunofluorescence experiments showed that MSNs-FA nanoparticles (green fluorescence) could penetrate from cytomembrane to cell interior by FR-mediated cell endocytosis, and accumulate strongly in cytoplasm with incubation time prolonged from 12 h to 24 h. N9 with red fluorescence labeling was able to reach mitochondria and specifically bound with Bcl-2 protein after 12 h of incubation with the carrier of FA-targeted MSNs, the interaction effect became more obvious especially at 24 h, which could be seen from the merged fluorescence colors (Fig. 3B). The interaction between N9 and Bcl-2 will pave the way for converting the anti-apoptotic function of Bcl-2 in targeted cancer therapy.

### 2.5. Bcl-2-depdent co-localization of peptide with mitochondria

To examine whether mitochondria targeting by N9 peptide was dependent on Bcl-2 expression, we carried out the similar experiments in Bcl-2 gene-knocked out- HeLa cancer cells. The intracellular localization behavior was examined corresponding to different incubation times. Confocal images showed that N9 peptide accompanied with FA-modified MSNs could accumulate in cells with time prolonged from 1 h to 24 h. The accumulation level on cytoplasm could be distinguished either from the distance between N9/MSN and mitochondria, or the merged yellow fluorescence intensities. We found that the intracellular fluorescence intensity was enhanced with incubation time increased, and the distance with mitochondria was reduced. However, the co-localization of N9 with mitochondria wasn't present even at 24 h (Fig. 4). N9 peptide was more close to mitochondria with time prolonged, however, it couldn't arrive the mitochondria without the presence of Bcl-2. The above phenomenon collectively demonstrated that the expression of Bcl-2 was necessary for N9 peptide in mitochondria targeting and even the final apoptotic effects. Bcl-2 is a major target of N9 peptide.

### 2.6. Inhibitory effects on cancer cell growth in vitro

To assess the selective cytotoxicity of N9@MSNs-FA, FA-positive HeLa or negative HEK293T cells were treated with free N9, N9-loaded MSNs-FA with vary concentrations (1-200 μg/ml) for 48 h to evaluate the effects on cell proliferation. For comparison, N9 without cell-penetrating peptide (CCPs) domain was used as the positive control. It was found that free N9 hardly changed the cell activity due to its inaccessibility to cell interior. In contrast, the substantial inhibition of cell proliferation was largely associated with the N9-loaded MSNs-FA (Fig. 5A-B). The results showed that the viability of HeLa cells could be effectively decreased by N9-loaded MSNs-FA in a dose-dependent

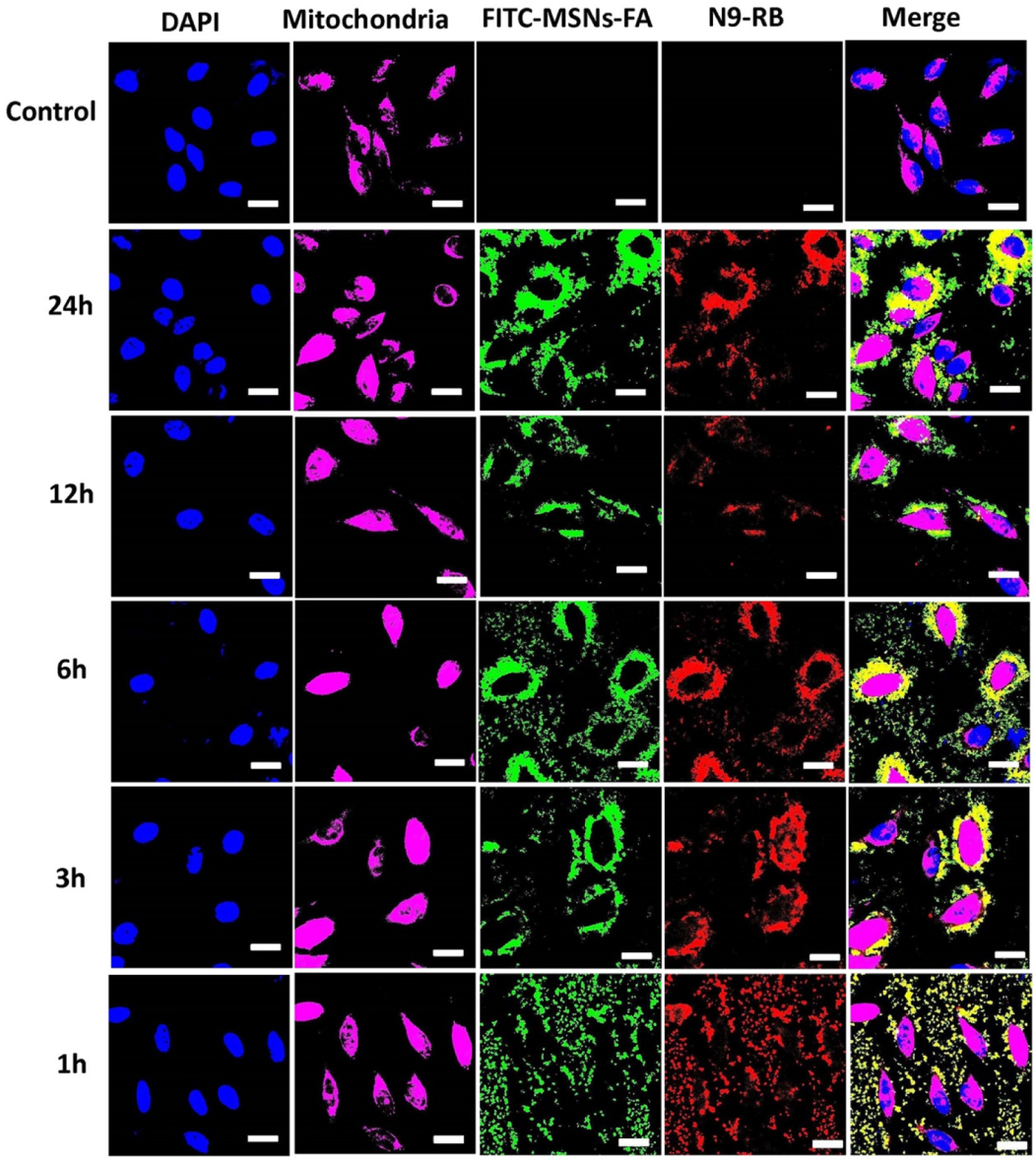


**Fig. 4.** The Bcl-2-dependent co-localization behaviors of N9-RB@FITC-MSNs-FA nanoparticles with mitochondria in Bcl-2 gene-knock out HeLa cells at different incubation time intervals. Scale bar: 25 μm.

manner. When the concentration of N9@MSNs-FA was increased from 1 to 200 μg/ml, the viability of HeLa cells was decreased sharply from about 94.3% to 24.6% (Fig. 5B). As expected, N9-encapsulated MSNs-FA had no apparent effect on HEK293T cell growth (Fig. 5A). The reason why N9@MSNs-FA showed little improvement on the proliferation of HEK293T cells might be deemed to the low expression of folate receptor on cell membrane. When converting the action concentration of MSNs to the corresponding actual concentration of N9 based on the respective loading efficiency, N9 with the delivery of MSNs-FA at the relatively less action concentrations had the more effective inhibitory effects on HeLa cells not HEK293T cells. The IC50 value of N9@MSNs-FA against HeLa cells was 32.83 μg/ml (equivalent to 2.54 μM N9), which was nine times less than that against HEK293T cells, further demonstrating the effective proliferation-inhibition capability of nanodrugs on target cancer cells. These results collectively confirmed that N9 could be intracellularly delivered by MSNs-FA with great selectivity.

### 2.7. Flow cytometric analysis of cell apoptosis

To evaluate the apoptosis effects of N9-encapsulated MSNs-FA on HeLa cells, flow cytometric analysis was carried out on a Beckman Coulter cytoflex with Annexin V-FITC/PI double staining method. The percentage of apoptotic cells after 48 h-treatment with N9 or N9@MSNs-FA was quantitatively calculated based on cells labeled with Annexin V-FITC and/or PI in the sample groups relative to control one. It was found that free N9 almost didn't produce cell apoptosis (3.7%), which still kept more than 73% of survival for HeLa cells (Fig. 5C). In contrast, on the normalization of N9 dose, N9-encaspulated MSNs-FA displayed the discrepant anti-proliferation efficiency mediated by the FA molecule on MSNs and the specific interaction between N9 and intracellular Bcl-2 protein. When the concentration of N9@MSNs-FA was 100 μg/ml, the total percentage of the apoptotic HeLa cells was 51.66% compared to control. Unexpectedly, N9 and N9@MSNs-FA didn't show any apoptosis-inducing effect on HEK293T cells (Fig. 5C). The above results demonstrated that MSNs-FA nanocarriers could take actions in the final inhibitory effects of N9 on target cancer cell activity.

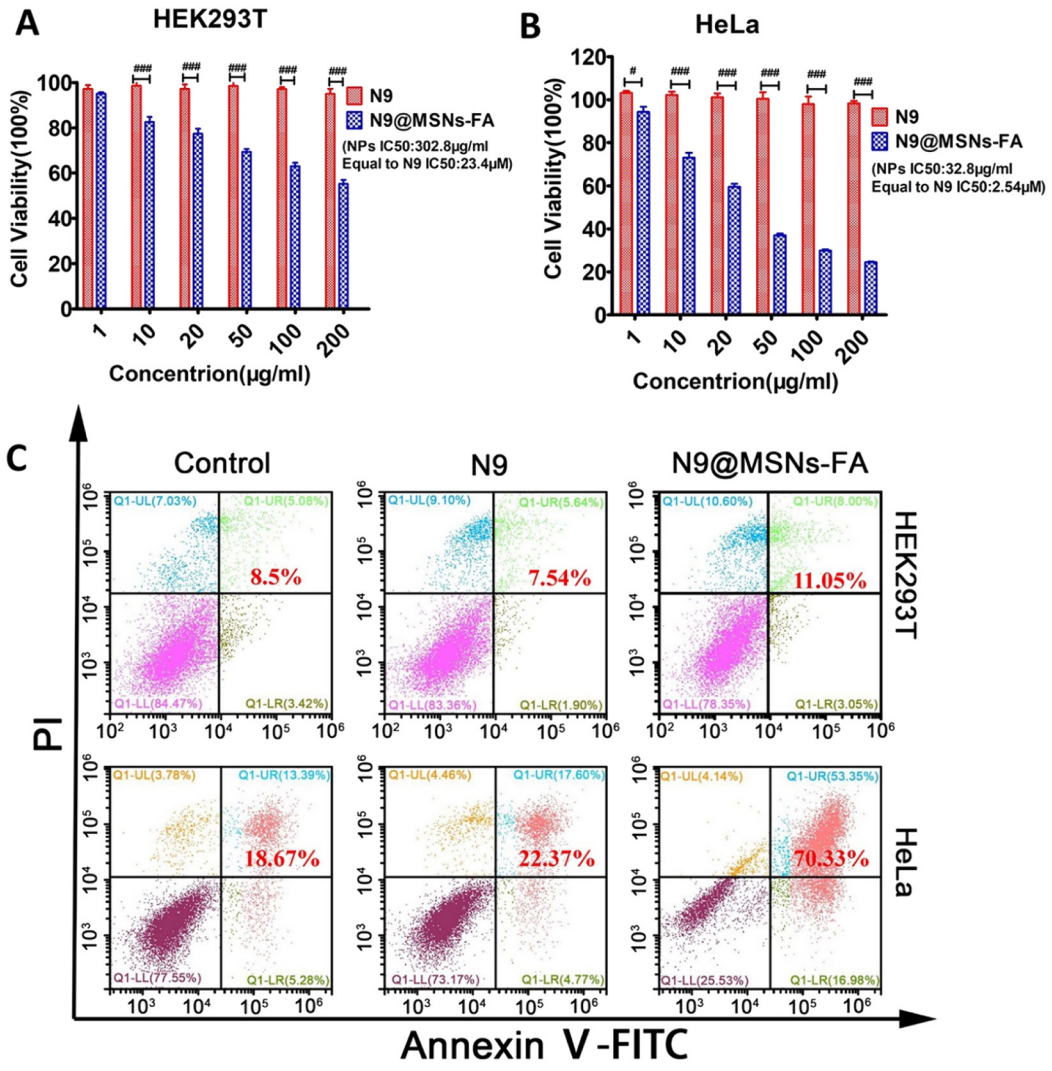


**Fig. 5.** The effect of N9 peptide on cell activity with the delivery of MSNs-FA nanoparticle. The selective cytotoxicity of N9-loaded MSNs-FA nanoparticles to FR-negative (HEK293T, A) and positive cells (HeLa, B) at various nanoparticle concentrations ranging from 1 to 200 μg/ml after 48 h exposure. The comparison was made between free N9 and N9@MSNs-FA. Symbol ($^{###}$) indicates the very significant difference, $p < 0.001$. C, Analysis of the apoptotic effects on HEK293T and HeLa cells selectively induced by N9-loaded MSNs-FA (100 μg/ml) nanoparticles after 48 h incubation. In these assays, free N9 peptide was used as the positive control.

### 2.8. Biosafety in Zebrafish models

Zebrafish embryos rather than mammalian models were employed to evaluate the bio-toxicology of these functional MSNs [17-19], which allowed the evaluation of the possible effects on lethality (acute toxicity) and hatchability. The acute assay was performed by incubating 20 zebrafish embryos of 48-hpf with MSNs-$NH_2$ or MSNs-FA nanomaterials in three different concentrations for measurement of the cumulative mortality until at 72 h. It was clear that it might be safe for naked MSNs-$NH_2$ nanoparticles below the dose of 200 μg/ml, but at 200 μg/ml MSNs-$NH_2$ induced the zebrafish embryo to be dead in an incubation time-dependent manner. The mortality rate reached 80% at 72 h. In sharp contrast, after surface decoration with FA, MSNs-FA nanoparticles produced the less toxic to zebrafish embryos than MSNs-$NH_2$, which kept approximately 70% of embryo alive even after 72 h exposure (Fig. 6A-C). Besides, the hatching rate was significantly improved by MSNs-FA compared to MSNs-$NH_2$. The Zebrafish embryos treated with MSNs-FA nanoparticles hatched 70% at 72 h while only 20% embryos hatched in the MSNs-$NH_2$-treated embryos (Fig. 6D). Overall, the MSNs-FA nanoparticles as nanocarriers displayed the great biosafety *in vivo*, which might be due to the biocompatible components (e.g., FA) present on MSNs surface [20].

## 3. Discussion

Various stimuli-responsive multifunctional MSNs were developed as drug nanocarriers for effective cancer therapy [21,22]. However, compared to the conventional small pore-sized MSNs, the large pore-sized MSNs exhibited the superior advantages on facilitating the cell penetration and realizing the subcellular site-specific delivery of biomacromolecules (therapeutic peptide, protein, and nucleic acid) [23,24]. In this study, we report the unique MSNs with macropores of 10-15 nm in diameter and successfully encapsulate a Bcl-2-converting peptide (N9) into the pores with the loading efficiency of 8.2% (Fig. 1). HeLa cells with elevated Bcl-2 and FR expression were selected as the targeted cancer model *in vitro*. The surface functionalization of MSNs with FA displayed the FR-mediated cancer cell targeting and endocytosis effects in HeLa cells (Fig. 2), which was similar as what previously reported [12,13,25]. Besides, the amino groups of MSNs nanoparticles were protonated at acidic endosomal pH, which disrupted the endosome and promoted the escape of particles from endosome into cytoplasm. The escape behavior was attributed to the “proton-sponge”

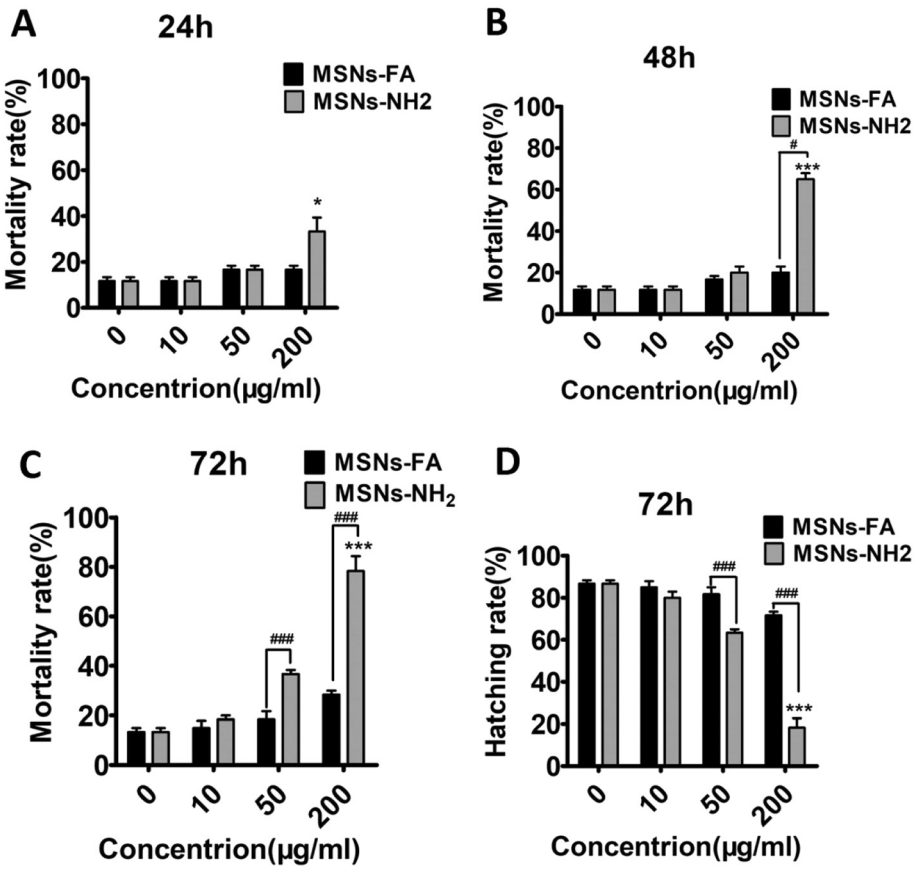


**Fig. 6.** Measurements of the *in vivo* biosafety of free nanocarriers using zebrafish model. The mortality rate of zebrafish embryos after individual incubation with MSNs-$NH_2$ and MSNs-FA nanoparticles at concentrations ranging from 10 to 200 μg/ml for 24 h,48 h or 72 h (A, B, C). The hatching rate of zebrafish embryos after 72 h of exposure to various concentrations of MSNs-$NH_2$ and MSNs-FA nanoparticles (D). The significance analysis was performed on the basis of the control (*) or MSNs-NH2 nanoparticles ($^{\#}$). Symbols (*, $^{\#}$) and (***, $^{\#\#\#}$), respectively, indicate statistically significant and very significant difference.

or "endosome buffering" effects [26,27], which largely contributed to the mitochondrial localization of the delivered N9 peptide by the above functional MSNs (Fig. 3). Moreover, the mitochondrial localization is a Bcl2-dependent manner (Fig. 4), which paved the way for the final cell apoptosis effects (Fig. 5) via the specific interaction between N9 peptide and Bcl-2 protein [6]. Besides, the *in vivo* biosafety of MSNs is another key factor that limits its application. Various means were taken to reduce the severe and unpredictable toxicity risks including introduction of disulfide bonds into the silica framework to achieve a stimuli-responsive biodegradation [28,29], or surface functionalization of MSNs with biocompatible molecules to improve the biocompatibility. The substitutes for CPPs by the functional MSNs avoided of the toxic side effects of carriers and the non-selective transport of the delivered drugs [3,30], which was both demonstrated in *in vivo* zebrafish embryo assays (Fig. 6) and the *in vitro* cell targeting assays (Fig. 2). Zebrafish has been widely recognized as an *in vivo* organism model for evaluating the nano environment and human safety (EHS). The unique characters, such as embryo transparency, high fecundity, low cost and short reproduction time, potentiate zebrafish to be a model between the traditional cell culture and mammalian [17-19]. The zebrafish assays not only provide the validation for *in vitro* cell toxicity, but also the reference for *in vivo* animal experiments. Thus, zebrafish was selected as a fast and valid *in vivo* model to evaluate the biosafety of MSNs-FA nanoparticles in this study. Collectively, our study demonstrated that the functional MSNs with macropores had the significant promise in delivering peptide or protein drugs for targeted cancer treatment. In spite of various nanoformulations such as PLA-PEG-PPG-PEG tetrablock copolymer [3,31], iron oxide-based nanoparticles (SPIONs) [30] and polyhydroxybutyrate based nanoparticles (PHB-PEG) [32] were developed for intracellular delivery of N9 peptide to treat cancer, employment of the dual targeting inorganic silica nanoparticles with macropores as the novel carriers hasn't yet been reported. In comparison with the above nanoformulations, our delivery system showed the excellent anticancer efficacy with great *in vivo* biosafety.

## 4. Conclusions

To be concluded, the novel macroporous silica nanoparticle platform functionalized with folic acid was constructed by us for delivering the Bcl-2-function converting peptide to treat cancer cells. The delivery system had the dual functions with cancer cell membrane targeting using FA-coupled MSNs and mitochondrial binding with the intracellular delivery of the anti-cancer drug N9. The MSNs-FA nanoparticles showed great *in vivo* biosafety compared to the naked MSNs without surface modification, which led to only less than 30% zebrafish embryos to death even after 72 h of exposure. With the employment of MSNs-FA nanocarriers, the cell-penetrative capabilities of N9 peptide seemed to be largely enhanced with great selectivity, with over 50% apoptotic HeLa cells after 48 h of co-incubation. In a word, the functionalized macroporous silica nanoparticles with tumor targeting effects were successfully synthesized, which brought out the intracellular delivery of Bcl-2-converting peptide in cervical cancers with great specificity and biosafety. Our design could not only solve the difficulty in intracellular delivery of therapeutic peptides to tumors, but also increase the unique activities and functions of such hydrophilic biomacromolecule drugs. This study will provide the design strategy for functional nanoparticles to solve the defects of therapeutic peptide/protein drugs in cancer application.

## 5. Experimental section

### 5.1. Materials

FITC (purity, 96%) was purchased from Shanghai Macklin Biochemical Co. Hexadecyl trimethyl ammonium chloride (CTAC, ≥98%) was purchased from Sinopharm Chemical Reagent Co. 3-

Aminopropyltriethoxysilane (APTES, ≥98%), Tetraethyl orthosilicate (TEOS, 98%), FA (≥97%), 1-(3-Dimethylaminopropyl)-3 -ethylcarbodiimide hydrochlorid (EDC), N-Hydroxysuccinimide (NHS, 98%), DAPI and [3-(4,5-dimethylthiazol-2-yl)-2,5-diphenyltetrasodium bromide] tetrazolium salt (MTT) were obtained from Sigma-Aldrich. TEA (≥98%) was purchased from Aladdin. Bcl-2-converting peptide with or without FITC labeling (FSRSLHSLL, N9 or N9-FITC, ≥98%) was synthesized and purified by LifeTein (Beijing) Ltd, and N9 with RB labeling (N9-RB) was from GL Biochem (Shanghai)Ltd. MitoTracker® Red and Deep Red dyes were purchased from Life Company. Pure water was used in all experiments. All other chemicals, unless otherwise specified, were all purchased from Sinopharm Chemical Reagent Co., Ltd and used without further purification.

### 5.2. Preparation and characterization of functional MSNs before and after therapeutic peptide loading

#### 5.2.1. Synthesis of MSNs and amino-modified MSNs

The large pore sized-MSNs were synthesized as we previously reported [10,33], followed by the surface modification with amine groups. Specifically, MSNs were dispersed in 50 ml of ethanol and refluxed for 4 h at 80-90 °C water bath, followed by the addition of 300 μl APTES refluxed for another 24 h. Amine-modified MSNs were obtained after repeated centrifugation and washing with ethanol and water to remove the unreacted APTES and finally dispersed in water for lyophilization.

#### 5.2.2. Synthesis of FA-functionalized MSNs loaded with therapeutic peptide

To obtain the functionalized MSNs with the ability of tumor targeting, FA was covalently attached onto the surface of MSNs prior to the loading of N9 peptide. FA (2 mg) dissolved in 4 ml of DMSO were treated with excess molar ratios of EDC and NHS for 2 h in dark. The active ester of FA was then mixed with the amine-terminated MSNs (20 mg) in the mixed solution of 6 ml of DMSO and 18 ml of DMF under vigorous stirring for 24 h. The FA-attached MSNs were finally obtained by repeated washing to remove the unreacted FA, and the excess EDC, NHS, DMF and DMSO.

Anticancer peptide N9 was then conjugated onto the MSNs-FA surface or loaded into the macropores of MSNs-FA. For the synthesis of N9-MSNs-FA conjugates, N9 peptide was firstly dissolved in PBS (pH 7.4), and mixed with equal molar ratios of EDC and NHS for stirring. After 1 h of activation, the N9 peptide solution was added with MSNs-$NH_2$ reacting for another 24 h at 25 °C. Excess EDC, NHS and N9 were then removed by repeatedly washing and centrifugation with $ddH_2O$ for several times. The conjugates were finally dispersed in water and stored at 4°Cfor use. For the preparation of N9@MSNs-FA, the traditional double emulsion/solvent evaporation (W/O/W) method was used. 1.4 mg of MSNs-FA was added into N9 solution in PBS (pH7.4) with a mass ratio of $M_{(N9)}$:$M_{(MSNs\text{-}FA)}$ in 1:3 at room temperature stirring for 24 h in dark. After the reaction was completed, the mixture was centrifuged at 14,000 rpm for 30 min, the supernatant was collected and the precipitate was washed with $ddH_2O$. The above supernatant after centrifugation was measured for the content of N9 by the BCA assay as previously reported [32], and the drug loading of MSNs-FA was calculated based on the obtained value. The encapsulation efficiency (EE) and loading efficiency (LE) of N9 were calculated based on the following equations (1) and (2), respectively:

$$\%EE = \frac{Initial\ amount\ of\ N9 - Amount\ of\ N9\ in\ supernatant}{Initial\ amount\ of\ N9} * 100\% \quad (1)$$

$$\%LE = \frac{Initial\ amount\ of\ N9 - Amount\ of\ N9\ in\ supernatant}{Amount\ of\ N9@MSNs - FA\ nanoparticles} * 100\% \quad (2)$$

#### 5.2.3. Release studies of N9 peptide from MSNs-FA nanoparticles

The release of N9-FITC from the macropores of MSNs-FA nanoparticles was performed in PBS solutions with pH values at 7.4, 6.8, and 5.0. N9-FITC@MSNs-FA nanoparticles (3.2 mg) at the N9 concentration of 0.656 mg/ml were respectively dialyzed in the above PBS solutions (3 ml) and shaken in an incubator at 37 °C, 300 rpm to simulate the physiological environments. At different time intervals (2, 4, 6, 10, 24, 48, 96 h), the dialysate (0.02 ml) was taken out and transferred for the ultraviolent measurement at the wavelength of 490 nm on a microplate reader (Promega Glomax ® Discover). At the same time, the same volumes of PBS solutions (0.02 ml) with different pH values were replenished to the corresponding N9-FITC@MSNs-FA solutions to keep the total volume of the mixture constant. The curve of cumulative release percentage versus time was finally plotted based on the measured results and the standard curve of N9-FITC solution.

#### 5.2.4. Synthesis of FA-modified MSNs labeled with FITC

Briefly, FITC (1 mg) was dissolved in 1 ml of DMSO, and reacted with MSNs-FA(4 mg) under vigorous stirring overnight in dark. 1 M $NaHCO_3$ was used to keep the reaction solution at pH 8.5. FITC-labeled MSNs were then collected by centrifugation and washing with DMSO and $ddH_2O$ for several times to remove the unreacted FITC. Finally, the powder of MSNs-FITC was obtained by lyophilization.

#### 5.2.5. Characterization of N9-loaded MSNs-FA nanoparticles

To confirm the successful conjugation of FA onto the surface of MSNs, $^1H$ NMR spectra was made on a Bruker 600 MHz spectrometer to show the characteristic proton peak of FA in DMSO-$d_6$ (dimethyl sulfoxide-d6) or MSNs-FA in $CDCl_3$. DLS measurements were performed on a Nano Zetasizer setup (Nano ZS90) to show the change in hydrodynamic diameters (diameter, nm) and surface charges (zeta potential, mV) of MSNs nanoparticles in pure water before and after different surface functionalization at the same concentration of 100 μg/ml. The SEM and TEM images were respectively taken on a field emission scan electron microscope (Zeiss, SUPRA 55) at 5.00 kV and a TEM (TecnaiG2 Spirit BioTwin) at 200 kV to determine the surface morphologies and particle sizes of MSNs before and after FA attachment and N9 loading. The dendrimer-like mesoporous structures of MSNs nanoparticles were also observed from the SEM and TEM images. The large pore size characters of MSNs were then determined by the nitrongen adsorption-desorption isotherms, which were measured on a Micrometitics Tristar II 3020system and calculated both by the BarretteJoynereHalenda (BJH) and Brunauer_Emmett_Teller (BET) methods. The fluorescence images were also taken under a fluorescence inverted microscope (Zeiss Axio Observer A1) to further verify whether RB-labeled N9 peptide was successfully encapsulated into the macropores of FITC-labeled MSNs-FA nanoparticles.

### 5.3. Cell culture

Human cervical cancer HeLa cells and Human emborynic kidney HEK293T cells were respectively cultured in MEM and DMEM mediums supplemented with 10% fetal bovine serum, 100 units/ml penicillin, and 100 mg/ml streptomycin. All the cell lines above were grown at 37°Cin a humidified atmosphere of 5% CO2 incubator. When reached the confluence of 70-80%, cells were harvested using 0.25% trypsin and re-suspended in fresh medium for subsequent experiments.

### 5.4. Selective and competitive binding of FITC-MSNs-FA nanoparticles

To confirm the binding specificity of FA-coated MSNs to target cancer cells, FR-positive and negative HeLa and HEK293T cells were used in this assay. The adherent cells on coverslip-coated 24-well plates were respectively incubated with FITC-labeled MSNs-FA nanoparticles. After 1, 3, 6, 12 h interval times, cells were washed with PBS, stained with mitotracker (Red or Deep red) and nuclear dye DAPI (blue) in dark

and finally imaged under a confocal microscope. The specific binding and internalization behaviors of FA-coated MSNs in response to various cell lines were evaluated by the green fluorescence intensity from cells.

The FR-mediated binding and endocytosis behaviors of FITC-MSNs-FA nanoparticles were further verified by the competitive assays. HeLa cells were seeded on a 6-well plate at $5 \times 10^5$ cells/well. After 24 h of attachment, cells were treated with free FA (7.5 μM) prior to the incubation of FITC-MSNs-FA nanoparticles for different time periods (3, 6, 12, 24 h). Then cells were washed with PBS to remove the excess nanoparticles. All the cells were collected after trypsinization and centrifugation, and used for flow cytometric analysis. The cellular uptake efficiency was finally decided by the percentage of FITC-positive cells related to the control.

### 5.5. Microscopic analysis of the intracellular localization of peptide-loaded MSNs-FA nanoparticles

HeLa cells were treated with fluorescence-labeled N9@MSNs-FA nanodrugs (N9-RB@FITC-MSNs-FA, 33 μg/ml) for 12 h or 24 h prior to the staining procedures. Then cells were washed several times with PBS and treated with deep red-mitochondrial tracker for 45 min at 37 °C under dark condition. After removal of the staining solution, cells were then fixed with 4% paraformaldehyde at 25 °C for 10 min, and stained with DAPI solution (5 μg/ml) in PBS for 15min. The treated cells with N9-RB@FITC-MSNs-FA could be also pre-fixed with 4% paraformaldehyde for 10 min, followed by incubation with 0.2% Triton X-100 for 5 min, with 3% BSA for 30min, and then with fluorescence-labeled antibody against the intracellular protein Bcl-2 (deep red) for 2 h at 37 °C condition. The cell nucleus was similarly labeled with DAPI. Finally, all the above cell samples were observed by a laser confocal microscope. The intracellular localization behaviors of N9-RB@FITC-MSNs-FA with mitochondria or Bcl-2 protein could be clearly decided by the merged fluorescence colors and coincidence areas.

### 5.6. Bcl-2-dependent localization of N9 peptide with mitochondria

Whether the localization of N9 peptide with mitochondria was in a Bcl-2-dependent way was further determined by using Bcl-2 gene-knocked out HeLa cells (Bcl-$2^{-/-}$ Hela). The Bcl-$2^{-/-}$ HeLa cells were obtained in our laboratory as we previously reported. The procedures about the cellular internalization were similarly taken as above. HeLa cells were incubated with a certain concentration of N9-RB@FITC-MSNs-FA nanodrugs at 37 °C for 1, 3, 6, 12, 24 h. Then the medium was replaced with preheated (37 °C) medium containing mitotracker. After incubation for 30 min, the cells were washed with PBS and fixed with 4% paraformaldehyde, and stained with DAPI solution (5 μg/ml) in PBS for 15min. After serval times with washing, the cells were monitored under a laser confocal microscope (Zeiss Exciter 5).

### 5.7. Anticancer efficacy of N9@MSNs-FA nanodrugs

The *in vitro* anticancer efficacy of N9@MSNs-FA nanodrugs to HeLa and HEK293T cells were respectively determined using the MTT assay. Free N9 peptide was used as the positive control. The cells were seeded onto 96-well plate at a density of $5 \times 10^3$ cells/well in a complete MEM and DMEM medium supplemented with 10% FBS in a humidified 5% CO2 atmosphere at 37 °C for 24 h. Then the cells were treated with fresh culture medium containing either free N9 or N9@MSNs-FA at different MSNs doses ranging from 1 to 200 μg/ml (equivalent to N9 concentrations from 0.08 μM to 15.7 μM). The cells were further incubated for 48 h, and then washed with PBS to remove excess samples. The cells were followed by incubation with MTT working solution (100μl/well, 200 μg/ml) at 37 °C for another 4 h. Finally, the viability of cells induced by N9 or N9@MSNs-FA was determined by the optical absorption values at the wavelength of 490 nm on a microplate reader (Promega Glomax ® Discover) and expressed as the percentage of A490 nm of the treated group compared to that of the untreated group.

### 5.8. Quantitative analysis of cell apoptosis

Annexin V-FITC apoptosis detection kit (Thermo Fisher Scientifc, Waltham, MA, USA) was used to quantify the apoptotic and necrotic cells by a standard fluorescence activated cell sorting (FACS) assay. HEK293T and HeLa cells were seeded onto 6-well plate on the confluence of 70%-80%, and treated with fresh culture medium containing either free N9 or N9@MSNs-FA at the same peptide dose of 8.2 μg/ml (7.8 μM) for 48 h. Then cells were routinely collected, washed twice with cold PBS, and re-suspended in lX binding buffer to $1 \times 10^6$ cells/ml. All the cells were stained with 500 μl of binding buffer containing 5 μl of FITC Annexin V solution and 5 μl of PI at room temperature for 15 min in the dark. Finally, the cells were detected on a Beckman Coulter cytoflex within 1 h. The total apoptosis rate of N9 or N9@MSNs-FA was analyzed using Flowjo software system and calculated both by the percentages of $FITC^+PI^-$ - and $FITC^+PI^{+-}$- cells in early and late apoptotic status.

### 5.9. Toxicity assessment of nanocarriers using zebrafish models

#### 5.9.1. Zebrafish husbandry

The zebrafish husbandry was performed as previously reported [34,35], and all the zebrafish experiments were carried out in accordance with the recommendations in the Guide for the Care and Use of Laboratory Animals of Xiamen University, China.

#### 5.9.2. Specific experimental methods

The normal fertilized and full-shaped fertilized zebrafish embryos were selected under a stereomicroscope (Guiguang, China) and randomly divided into eight groups (20 embryos/well, two duplicates) as reported [36] prior to systemic toxicity testing. MSNs nanoparticles before and after FA modification (MSNs-$NH_2$ and MSNs-FA) were respectively diluted into different concentrations (10, 50, 200 μg/ml) with standard dilution water. The above nanoparticles were added into each well of the 12-well cell culture plate and cultured in a thermostatic incubator at (27 ± 1) ° C for different time intervals. At the designated time points (24, 48, 72 h), the alive and dead embryos and the hating larvaes were recorded. Finally, the biological safety of the above MSNs nanoparticles against embryonic development of zebrafish was indicated by the mortality rates at 24-72 h, and the hatching rate at 72 h.

### 5.10. Statistical analysis

The statistical analysis was performed using Student's *t*-test and one-way analysis of variance (One-ANOVA) by the least significance difference (LSD) test (GraphPad Prism 5.0). The difference analyses were carried out between samples and control or any two samples, which were considered statistically significant (* or $^{\#}$) for p value $< 0.05$, significant (**or $^{\#\#}$) and very significant difference (***or $^{\#\#\#}$) for $p < 0.01$ and $p < 0.001$.

## Author's contributions

J.J. Xie conceived the study. J.J. Xie, P.J. Ge and Y.H. Wu designed the experiments. Y.H. Wu and P.J. Ge performed most of the experiments, W.X. Xu did some. M.Y. Li provided the zebrafish model and Q. Kang raised the zebrafish. J.J. Xie and Y.H. Wu analyzed and interpreted the data. J.J. Xie and Y.H. Wu wrote the original paper. J.J. Xie revised the paper. J.J. Xie, X.K. Zhang, and M.Y. Li provided the research fundings. All the authors have read and approved the final manuscript.

## Declaration of competing interest

None.

## Acknowledgements

This study was supported by National Natural Science Foundation of China (81702988, U1405229, 81672749, 91429306, 81670709), Natural Science Foundation of Fujian Province (2017J05137, 2017J01145), Regional Demonstration of Marine Economy Innovative Development Project (16PYY007SF17), Fujian Provincial Science and Technology Department (2017YZ0002-1), and XMU Training Program of Innovation and Enterpreneurship for Undergraduates (2018X0557, 2018Y0921).

## Appendix A. Supplementary data

Supplementary data to this article can be found online at https://doi.org/10.1016/j.msec.2019.110386.

## References

[1] Q. He, J. Shi, MSN anti-cancer nanomedicines: chemotherapy enhancement, overcoming of drug resistance, and metastasis inhibition, Adv. Mater. (Deerfield Beach, Fla.) 26 (2014) 391–411.
[2] J.C. Reed, Bcl-2-family proteins and hematologic malignancies: history and future prospects, Blood 111 (2008) 3322–3330.
[3] M. Kumar, D. Gupta, G. Singh, S. Sharma, M. Bhat, C.K. Prashant, A.K. Dinda, S. Kharbanda, D. Kufe, H. Singh, Novel polymeric nanoparticles for intracellular delivery of peptide Cargos: antitumor efficacy of the BCL-2 conversion peptide NuBCP-9, Cancer Res. 74 (2014) 3271–3281.
[4] M.H. Kang, C.P. Reynolds, Bcl-2 inhibitors: targeting mitochondrial apoptotic pathways in cancer therapy, Clin. Cancer Res. Off. J. Am. Assoc. Canc. Res. 15 (2009) 1126–1132.
[5] A.S. Azmi, Z. Wang, P.A. Philip, R.M. Mohammad, F.H. Sarkar, Emerging Bcl-2 inhibitors for the treatment of cancer, Expert Opin. Emerg. Drugs 16 (2011) 59–70.
[6] S.K. Kolluri, X. Zhu, X. Zhou, B. Lin, Y. Chen, K. Sun, X. Tian, J. Town, X. Cao, F. Lin, D. Zhai, S. Kitada, F. Luciano, E. O'Donnell, Y. Cao, F. He, J. Lin, J.C. Reed, A.C. Satterthwait, X.K. Zhang, A short Nur77-derived peptide converts Bcl-2 from a protector to a killer, Cancer Cell 14 (2008) 285–298.
[7] P. Yang, S. Gai, J. Lin, Functionalized mesoporous silica materials for controlled drug delivery, Chem. Soc. Rev. 41 (2012) 3679–3698.
[8] S.H. Wu, C.Y. Mou, H.P. Lin, Synthesis of mesoporous silica nanoparticles, Chem. Soc. Rev. 42 (2013) 3862–3875.
[9] L. Li, J. Ding, J. Xue, Macroporous silica hollow microspheres as nanoparticle collectors, Chem. Mater. 21 (2009) 3629–3637.
[10] W. Xu, P. Ge, B. Niu, X. Zhang, J. Liu, J. Xie, Macroporous silica nanoparticles for delivering Bcl2-function converting peptide to treat multidrug resistant-cancer cells, J. Colloid Interface Sci. 527 (2018) 141–150.
[11] P.S. Low, S.A. Kularatne, Folate-targeted therapeutic and imaging agents for cancer, Curr. Opin. Chem. Biol. 13 (2009) 256–262.
[12] W. Cheng, J. Nie, L. Xu, C. Liang, Y. Peng, G. Liu, T. Wang, L. Mei, L. Huang, X. Zeng, pH-sensitive delivery vehicle based on folic acid-conjugated polydopamine-modified mesoporous silica nanoparticles for targeted cancer therapy, ACS Appl. Mater. Interfaces 9 (2017) 18462–18473.
[13] L. Xiong, X. Du, F. Kleitz, S.Z. Qiao, Cancer-cell-specific nuclear-targeted drug delivery by dual-ligand-modified mesoporous silica nanoparticles, Small 11 (2015) 5919–5926.
[14] Y. Lv, Y. Cao, P. Li, J. Liu, H. Chen, W. Hu, L. Zhang, Ultrasound-triggered destruction of folate-functionalized mesoporous silica nanoparticle-loaded microbubble for targeted tumor therapy, Adv. Healthc. Mater. 6 (2017).
[15] L. Pan, Q. He, J. Liu, Y. Chen, M. Ma, L. Zhang, J. Shi, Nuclear-targeted drug delivery of TAT peptide-conjugated monodisperse mesoporous silica nanoparticles, J. Am. Chem. Soc. 134 (2012) 5722–5725.
[16] L. Pan, J. Liu, Q. He, L. Wang, J. Shi, Overcoming multidrug resistance of cancer cells by direct intranuclear drug delivery using TAT-conjugated mesoporous silica nanoparticles, Biomaterials 34 (2013) 2719–2730.
[17] A. Nel, T. Xia, H. Meng, X. Wang, S. Lin, Z. Ji, H. Zhang, Nanomaterial toxicity testing in the 21st century: use of a predictive toxicological approach and high-throughput screening, Acc. Chem. Res. 46 (2013) 607–621.
[18] S. Lin, Y. Zhao, A.E. Nel, S. Lin, Zebrafish: an in vivo model for nano EHS studies, Small 9 (2013) 1608–1618.
[19] V.E. Fako, D.Y. Furgeson, Zebrafish as a correlative and predictive model for assessing biomaterial nanotoxicity, Adv. Drug Deliv. Rev. 61 (2009) 478–486.
[20] Y. Chen, H. Chen, J. Shi, In vivo bio-safety evaluations and diagnostic/therapeutic applications of chemically designed mesoporous silica nanoparticles, Adv. Mater. (Deerfield Beach, Fla.) 25 (2013) 3144–3176.
[21] X.B. Xu, S.Y. Lu, C. Wu, Z.Y. Wang, C. Feng, N. Wen, M.Z. Liu, X.Y. Zhang, Z. Liu, Y.Q. Liu, C.Z. Ren, Curcumin polymer coated, self-fluorescent and stimuli-responsive multifunctional mesoporous silica nanoparticles for drug delivery, Microporous Mesoporous Mater. 271 (2018) 234–242.
[22] J.J. Liu, B.L. Zhang, Z. Luo, X.W. Ding, J.H. Li, L.L. Dai, J. Zhou, X.J. Zhao, J.Y. Ye, K.Y. Cai, Enzyme responsive mesoporous silica nanoparticles for targeted tumor therapy in vitro and in vivo, Nanoscale 7 (2015) 3614–3626.
[23] M. Wu, Q. Meng, Y. Chen, L. Zhang, M. Li, X. Cai, Y. Li, P. Yu, L. Zhang, J. Shi, Large pore-sized hollow mesoporous organosilica for redox-responsive gene delivery and synergistic cancer chemotherapy, Adv. Mater. (Deerfield Beach, Fla.) 28 (2016) 1963–1969.
[24] X. Du, S.Z. Qiao, Dendritic silica particles with center-radial pore channels: promising platforms for catalysis and biomedical applications, Small 11 (2015) 392–413.
[25] F. Porta, G.E. Lamers, J. Morrhayim, A. Chatzopoulou, M. Schaaf, H. den Dulk, C. Backendorf, J.I. Zink, A. Kros, Folic acid-modified mesoporous silica nanoparticles for cellular and nuclear targeted drug delivery, Adv. Healthc. Mater. 2 (2013) 281–286.
[26] T. Xia, M. Kovochich, M. Liong, H. Meng, S. Kabehie, S. George, J.I. Zink, A.E. Nel, Polyethyleneimine coating enhances the cellular uptake of mesoporous silica nanoparticles and allows safe delivery of siRNA and DNA constructs, ACS Nano 3 (2009) 3273–3286.
[27] Q. Zhang, F. Liu, K.T. Nguyen, X. Ma, X.J. Wang, B.G. Xing, Y.L. Zhao, Multifunctional mesoporous silica nanoparticles for cancer-targeted and controlled drug delivery, Adv. Funct. Mater. 22 (2012) 5144–5156.
[28] X. Du, F. Kleitz, X.Y. Li, H.W. Huang, X.J. Zhang, S.Z. Qiao, Disulfide-Bridged organosilica frameworks: designed, synthesis, redox-triggered biodegradation, and nanobiomedical applications, Adv. Funct. Mater. 28 (2018).
[29] X. Du, X.Y. Li, L. Xiong, X.J. Zhang, F. Kleitz, S.Z. Qiao, Mesoporous silica nanoparticles with organo-bridged silsesquioxane framework as innovative platforms for bioimaging and therapeutic agent delivery, Biomaterials 91 (2016) 90–127.
[30] M. Kumar, G. Singh, S. Sharma, D. Gupta, V. Bansal, V. Arora, M. Bhat, S.K. Srivastava, S. Sapra, S. Kharbanda, A.K. Dinda, H. Singh, Intracellular delivery of peptide cargos using iron oxide based nanoparticles: studies on antitumor efficacy of a BCL-2 converting peptide, NuBCP-9, Nanoscale 6 (2014) 14473–14483.
[31] D. Gupta, M. Kumar, P. Tyagi, S. Kapoor, A. Tyagi, T.K. Barman, S. Kharbanda, D. Kufe, H. Singh, Concomitant Delivery of Paclitaxel and NuBCP-9 peptide for synergistic enhancement of cancer therapy, Nanomedicine 14 (2018) 1301–1313.
[32] S. Kapoor, D. Gupta, M. Kumar, S. Sharma, A.K. Gupta, M.M. Misro, H. Singh, Intracellular delivery of peptide cargos using polyhydroxybutyrate based biodegradable nanoparticles: studies on antitumor efficacy of BCL-2 converting peptide, NuBCP-9, Int. J. Pharm. 511 (2016) 876–889.
[33] W. Xu, X. Gao, P. Ge, F. Jiang, X. Zhang, J. Xie, Dendrimer-like mesoporous silica nanospheres with suitable surface functionality to combat the multidrug resistance, Int. J. Pharm. 553 (2018) 349–362.
[34] M. Li, E.D. Dean, L. Zhao, W.E. Nicholson, A.C. Powers, W. Chen, Glucagon receptor inactivation leads to alpha-cell hyperplasia in zebrafish, J. Endocrinol. 227 (2015) 93–103.
[35] S. George, S. Lin, Z. Ji, C.R. Thomas, L. Li, M. Mecklenburg, H. Meng, X. Wang, H. Zhang, T. Xia, J.N. Hohman, S. Lin, J.I. Zink, P.S. Weiss, A.E. Nel, Surface defects on plate-shaped silver nanoparticles contribute to its hazard potential in a fish gill cell line and zebrafish embryos, ACS Nano 6 (2012) 3745–3759.
[36] J. Duan, Y. Yu, Y. Li, Y. Yu, Z. Sun, Cardiovascular toxicity evaluation of silica nanoparticles in endothelial cells and zebrafish model, Biomaterials 34 (2013) 5853–5862.